JOURNAL OF CATALYSIS 89, 256–266 (1984)

Nature and Localization of Poisoning Carbonaceous Matter in Reforming Catalyst Studied by Transmission Electron Microscopy

R. A. CABROL[1] AND A. OBERLIN

Laboratoire Marcel Mathieu, ER 131 du CNRS, UER Sciences, 45046 Orléans Cedex, France

Received January 18, 1983; revised May 4, 1984

Poisoning of Pt/γ-Al_2O_3 catalysts by carbonaceous matter has been studied by means of a conventional transmission electron microscope (TEM). Two locations of the same carbonaceous matter were found. First, small stacks of aromatic ring structures less than 10 Å in size are deposited more or less flat on the alumina crystal faces (the alumina individual crystal shape is an association of {111}, {110}, {100}, and possibly {112}). Then the same carbonaceous units gather to form porous carbon particles. Only the units localized upon alumina are assumed to form shells able to poison the catalyst by covering its surface.

INTRODUCTION

Naphtha reforming implies several reactions promoted by a bifunctional Pt/γ-Al_2O_3 or Pt-other metal/Al_2O_3 catalyst. It is well-known that the acid sites of alumina are mainly responsible for the cracking and isomerization of crude naphtha, while the metallic function acts in the hydrogenation–dehydrogenation, hydrogenolysis, and dehydrocyclization processes. Both functions are necessary also for isomerization and dehydrocyclization. At the same time, carbonaceous material is deposited on the catalyst, decreasing its activity and modifying its selectivity. This carbon can be considered as an undesirable product of reforming.

It has been stated that soon after the process starts a carbonaceous overlayer appears on Pt (*1*) and that some time later, the acid function of alumina is more affected by carbon deposition (*2*). The location and nature of this carbonaceous matter is almost unknown. The aim of the present work is to investigate the location of carbon relative to the catalyst and to characterize both products by means of a conventional transmission electron microscope (TEM). The principle is to image the catalyst and the carbon separately by means of dark-field techniques. It will be shown that very small stacks of aromatic ring structures (less than 10 Å in size) are deposited on the surfaces of the individual catalyst particles, thus forming a shell, whereas some of these carbon units gather also into porous aggregates a few thousand Ångstroms in size in the catalyst.

EXPERIMENTAL

Sampling

A Pt/γ-Al_2O_3–Cl catalyst containing 0.38% Pt and 0.9% Cl was used. It was prepared by impregnating samples of alumina Cyanamid Ketjen C.K. 300 following the method of Castro *et al.* (*3*). The specific area of the support was 200 m^2/g, the pore volume 0.48 cm^3/g, and the catalyst obtained had 82% dispersion as measured by the method of Benson and Boudart (*4*).

The runs to coke the catalyst were performed in bench-scale equipment that has already been described (*5*).

The following samples were prepared: (i)

[1] Present address: Instituto de Investigaciones en Catalisis y Petroquimica, INCAPE, Santiago des Estero 2954, 300 Santa Fe, Argentina.

0021-9517/84 $3.00

clean alumina; (ii) fresh catalyst; (iii) catalyst having been run under standard industrial conditions (P = 30 kg/cm^2, H_2/naphtha = 8, T = 758 K, WHSV = 6 h^{-1}) for a period of 500 h; the feed was a C_5–C_9 naphtha cut and the percentage of carbon at the end of the run was 1.5%; (iv) catalyst having been run under deactivation conditions, i.e., first a 7-h run during which the catalyst works at standard industrial conditions; then, the pressure is decreased to 10 kg/cm^2 and the hydrogen-to-naphtha ratio lowered to 4; finally a return to the initial values for the last 7 h. The feed was a C_{12}–C_{14} paraffin mixture and the carbon percentage at the end of the run was 6.8%; (v) fresh catalyst heated at 923 K in air for 6 h to sinter Pt; (vi) 6.8% coked catalyst heat-treated at 1173 K under vacuum.

TEM Techniques (EM 400 Philips Microscope with Ionic Pumping: Clean Vacuum).

A more or less crystalline material gives rise to at least one or a few scattered beams when it is struck by the incident electron beam inside the TEM. Each crystallite associated in a polycrystalline material gives rise to its own scattered beams specific to its relative orientation to the incident beam. If a given *hkl* beam of one crystallite is selected for imaging, the crystallite appears in the image as a bright domain in dark field (DF). Such techniques were developed and employed for a long time for identifying planar aromatic ring structures (*6, 7*). They do not need to be discussed here except for their principle. The aromatic structures are similar to small graphitic layers. Each of them (even single layers) gives rise to six 10 and six 11 scattered beams corresponding to the hexagonal symmetry. If such structures are piled up in parallel (even by 2), they give rise to an additional 002 beam corresponding to the interlayer spacing. The principle of the tilted dark-field mode was applied here for imaging both γ-alumina and carbon and, incidentally, sintered platinum.

In addition, lattice fringe techniques (abbreviated as LF) were applied also to alumina and carbon. They consist (*8*) in allowing a given *hkl* beam to interfere with the incident beam so as to obtain in the image bright and dark *hkl* fringes with the d_{hkl} period. Such an image visualizes the projection of the *hkl* family of lattice planes along the TEM optical axis. Since the Bragg angle for electrons is very small (~1° for 100 kV), the *hkl* images both in DF and LF correspond to families of planes nearly normal to the observation plane. More classical techniques were also used, such as selected area electron diffraction (SAD) and bright field (BF).

RESULTS

Alumina and Platinum

SAD patterns are Debye–Scherrer ones (Figs. 1a and b) showing dots when larger crystallites are present inside the field-limiting aperture. They show the normal succession of rings for γ-alumina with the expected intensities (see Table 1). The corresponding bright-field image (Fig. 1c) shows aggregates of very small individual particles more or less contrasted. This contrast arises from the fact that most of the alumina-scattered beams are withdrawn by the objective aperture set paraxial.

The darkest particles are thus single crystals fulfilling better the Bragg condition for one of the scattered beams withdrawn. Figures 2a, b, c show the radial exploration of

TABLE 1

ASTM Data for γ-Alumina

hkl	*d* (Å)	I/I_0
111	4.56	40
220	2.80	20
311	2.39	80
222	2.28	50
400	1.977	100
511	1.52	30
440	1.395	100

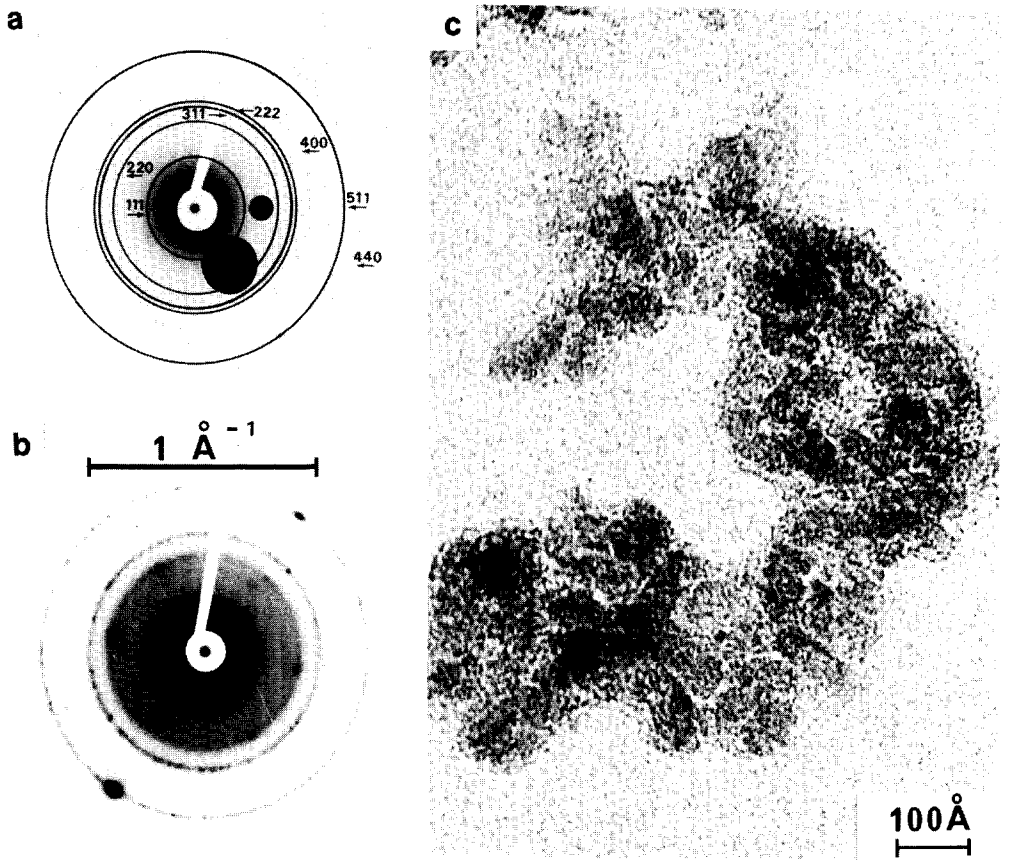

FIG. 1. (a) Schematic drawing of γ-alumina SAD pattern. (b) SAD pattern. (c) Bright field.

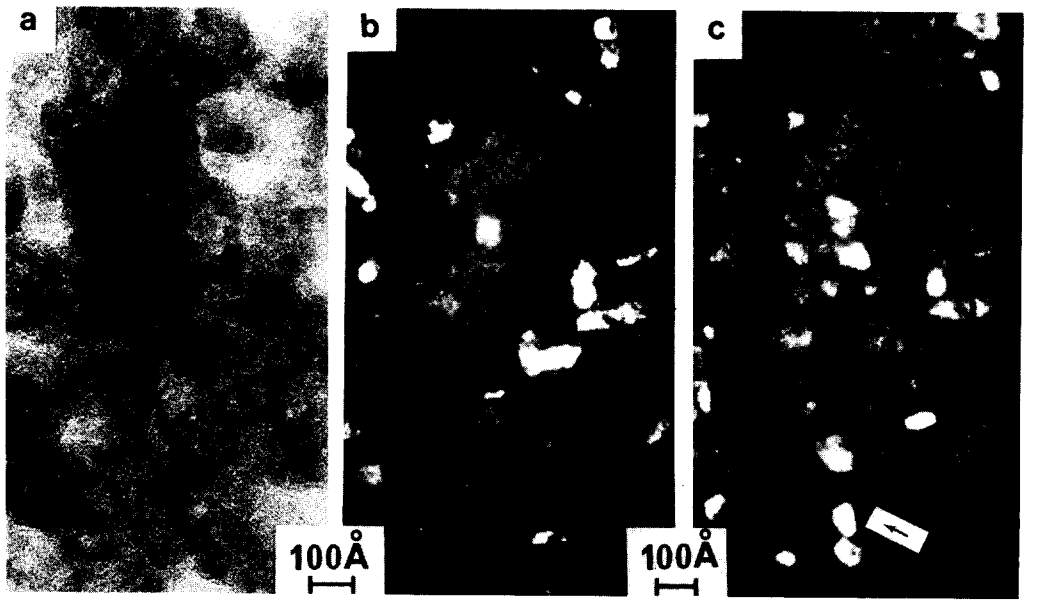

FIG. 2. Same field of a catalyst containing 6.8% of carbon. (a) Bright field, (b) 400 alumina dark field, (c) 440 alumina dark field.

the reciprocal space of alumina by a small aperture. This aperture is represented as the largest dark circle in the SAD pattern of Fig. 1a. Its diameter expressed in terms of the scattering vector $|\mathbf{s}| = 1/d_{hkl}$ is 0.20 Å^{-1}. Figure 2a is the bright field whereas Fig. 2b corresponds to 400 and Fig. 2c to 440 of alumina. Single crystals strongly light up in Fig. 2b whereas others become dark in Fig. 2c indicating different crystallographic orientations. If some single crystals remain lit up in both micrographs, it is probably because the aperture is too large to select only 400 or 440 and intersects also a portion of 311 or 222. Anyway, by comparing bright- and dark-field images it is demonstrated that each bright crystal in dark field corresponds to a single particle in bright field. It can be concluded that the aggregates observed are made of small single crystals 30–80 Å in size (the most frequent value is 50 Å).

Since such single crystals are very small, it is thus difficult to know what their crystalline shape is, i.e., which faces occur in their morphology. The Donnay-Harker law states that the external shape of a single crystal depends on the symmetry group of its atomic structure. For γ-alumina this group is O_H^7 (*10*). The succession of X-ray reflections is thus 111, 220, 311, 222, and 400. The corresponding solids are the octahedron {111}, rhombododecahedron {110}, trapezohedron {113}, and cube {100}. The external shape of a single crystal should be a combination of these four solids, but the more developed faces should be that of an octahedron. Despite the smallness of the single crystals we can restore the precise shape by using bright- and dark-field modes and lattice fringe imaging as well. An octahedron lying along (111) cannot give lattice fulfilling the 111 Bragg condition since all (111) planes are too much oblique (θ Bragg angles in electron diffraction are smaller than 2 or 3 degrees). Consequently all crystals lying on the (111) face will have an hexagonal outline and will be free of the 111 lattice fringes (4.56 Å in period). These crystals

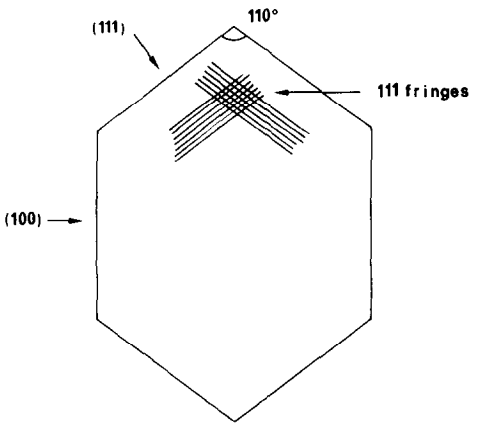

FIG. 3. Schematic drawing of the outline of a γ-alumina single crystal.

give only 440 reflections in their electron diffraction patterns; they will be recognized as those which are lit up in 440 dark field (see Fig. 2c). Crystals lying on the rhombododecahedron (110) face always give two families of planes fulfilling the 111 Bragg condition since such a crystal has two families of (111) planes perpendicular to the observation plane. All the crystals lying on (110) should give two sets of 111 fringes making the octahedron face angle, i.e., ~110° (see Fig. 4 in the center and Fig. 3). The general outline of the crystals will be an irregular hexagon with 110° and 130° angles (Fig. 3). It can be seen in Fig. 4 that when an angle in a particle containing fringes can be evaluated from its outline, it is always larger or smaller, but never equal to 120°. The occurrence of cube faces has to be assumed for explaining the angles of 110°. Figure 4 shows that the fringes are parallel to the edges of the particle since they make a 110° angle between them; this demonstrates that the corresponding edges are the projection of (111) octahedron faces (see Fig. 3). This is possible only if the hexagonal outline is completed by the profile of a cube face (100). Finally, many particles show only one set of fringes (see Fig. 4). There are two possibilities: either the crystal is misoriented by its neighbors or it lies on another face. Only (112) of a trapezohe-

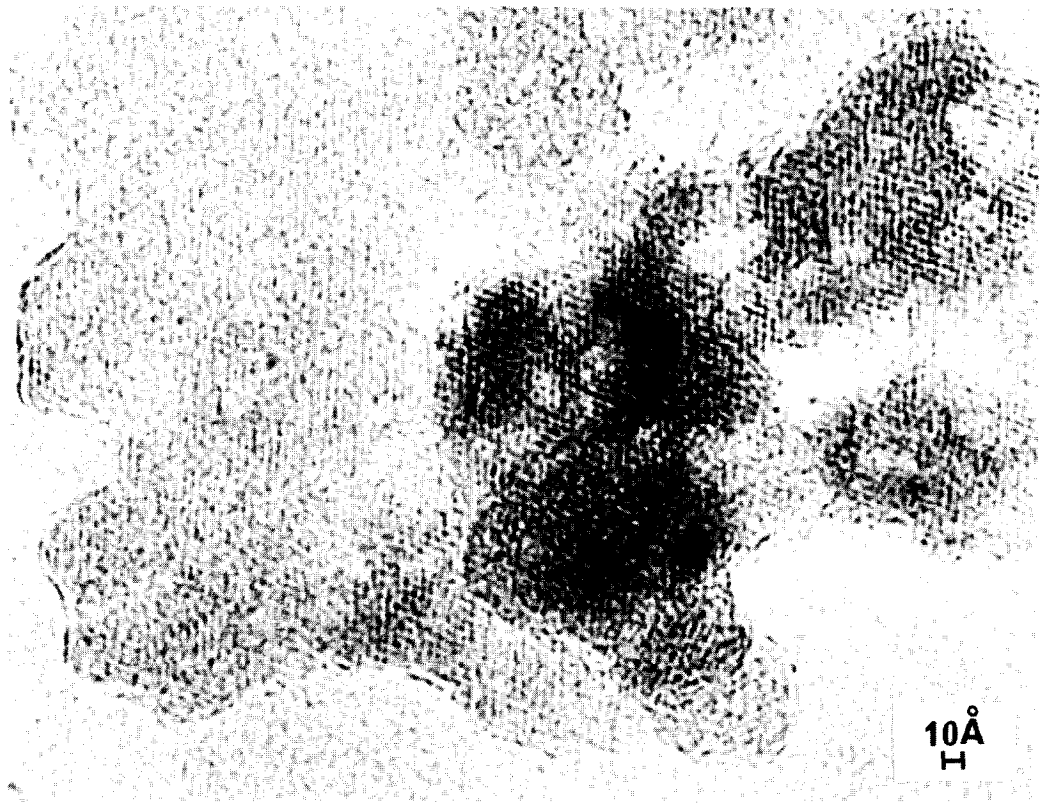

FIG. 4. Catalyst having run 500 h. 111 Alumina lattice fringes.

dron fulfills the 111 Bragg condition which brings $(\bar{1}\bar{1}1)$ alone perpendicular to the observation plane.

From such reasoning we may reasonably assume that particles have a composite shape made up of octahedron (dominating) and rhombododecahedron associated with relatively small facets of cube and trapezohedron.

Platinum deposited on the catalyst was not observed with certainty except for sintered samples heat-treated under vacuum at 1173 K. For most samples the alumina-scattered beams produced are too numerous for obtaining the platinum 111-scattered beam alone (see Table 1) in dark field, even with the smallest available objective aperture. Thus platinum crystals cannot be distinguished from alumina. However, in the heat-treated catalyst considered here and for an unknown reason, the beams scattered by alumina are so faint that individual platinum crystals light up very strongly in 111 Pt DF. By comparing these Pt particles to those observed in BF images of the 500-h run catalyst, it can reasonably be assumed that they are clusters of Pt (Fig. 5). Figure 5 corresponds to a part of a through-focus series demonstrating that the dark particles are not phase objects since they do not disappear as the focus is changed. In addition, such particles are found in a decreasing number when the samples observed become closer to the fresh catalyst. It is postulated that Pt exists in the fresh catalyst in a highly dispersed form that makes uncertain its identification over an alumina support.

Carbonaceous Matter

The scattered beams produced by any carbonaceous matter, even when it has a

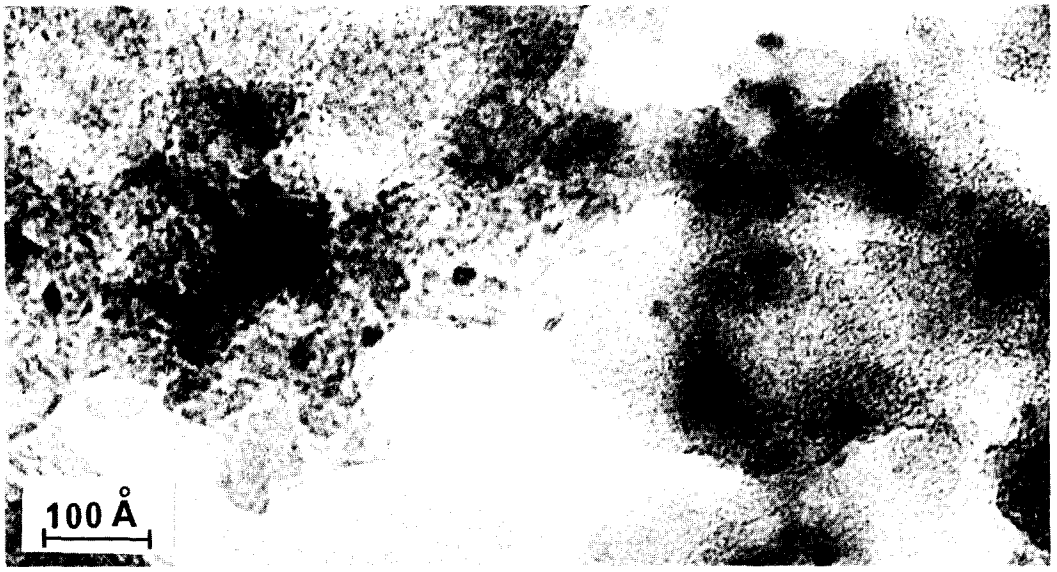

FIG. 5. Catalyst having run 500 h. Bright field showing clusters of platinum.

very poor crystalline organization, are at least those of aromatic planar structures whether single or piled up. If such structures are piled up by twos, the first scattered beam produced is the 002 one. It lies between $111_{Al_2O_3}$ and $220_{Al_2O_3}$. Figure 1 shows that 002 cannot pass alone through the large 0.20-$Å^{-1}$ aperture. It is always associated with $111_{Al_2O_3}$. However, $111_{Al_2O_3}$ is always very faint, since most of the particles tend to lie on their (111) faces. For all these particles the 111 reflection is missing in the SAD pattern. In the area delimited by the intermediate image aperture (diameter less than 1 μm) a majority of single crystals do not issue 111 beams for this reason. On the contrary, a majority of aromatic ring structures yield the 002 reflection. The 002 carbon DF images should thus be stronger than the alumina ones. The comparison between the BF and DF micrographs in Figs. 6a and b shows that the intense bright domains appearing in 002 carbon DF images first are localized differently and then have a much smaller size (~10 Å) than the alumina crystals (~30–80 Å). Some of them are localized around the outlines of the alumina small single crystal preferably to the faces parallel to the observation plane (insets in Fig. 6). Others are gathered in the particle marked by an arrow in Fig. 6a. Figure 6 is representative of the images corresponding to the sample containing 6.8% of carbon. It suggests the occurrence of two types of carbonaceous matter.

Decoration Around the Alumina Crystallites

The insets in Fig. 6, representing enlarged details of Fig. 6b, emphasize the positions of the bright domains as a decoration around the contours of the alumina single crystals. Each of these bright domains less than 10 Å in size could represent the image of aromatic planar ring structures less than 12 rings piled up by 2 or 3. Such units (basic structural units, BSU) are similar to those found in most carbonaceous materials (*6, 7*). Decoration around alumina crystals can be thus attributed to single BSU deposited on the alumina crystal faces (Fig. 7). DF images demonstrate that BSU lie preferably with their aromatic layers parallel to the alumina crystal faces since only those which are seen edge-on

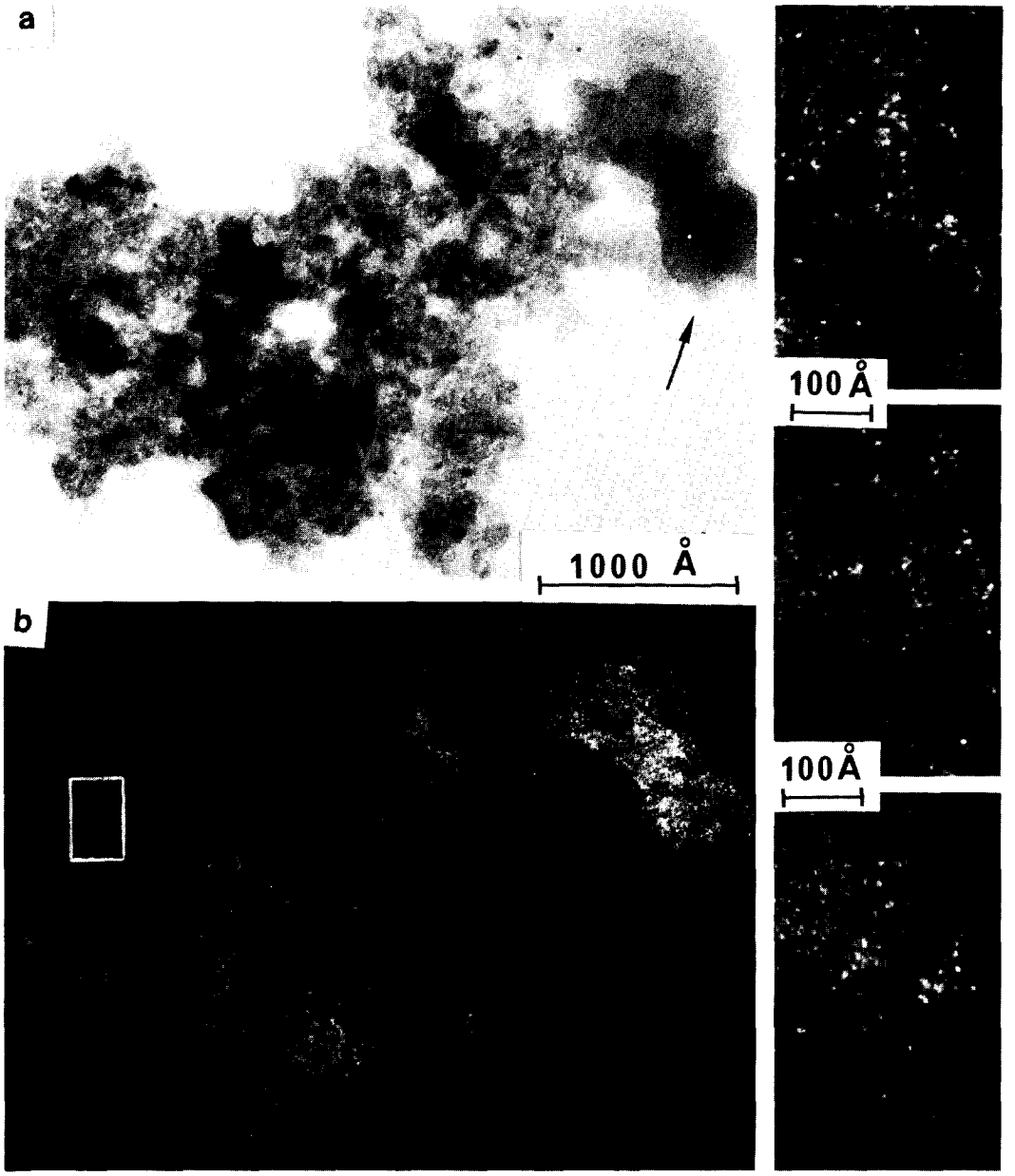

FIG. 6. Same field of a catalyst containing 6.8% of carbon. (a) Bright field, (b) 002 carbon dark field (insets are enlargements of details of Fig. 6b, the lowest one corresponds to the white square).

can be bright. In Fig. 7 the hexagonal outline only will be thus underlined by bright domains. Since the BSU lying on the alumina faces parallel to the observation plane do not fulfill the carbon 002 Bragg reflection, they are dark in the image. As the 0.20-$Å^{-1}$ aperture selects all the 002 beams of aromatic layers twisted $\pm 22°$, more than one edge of the irregular hexagons can be decorated by bright domains, especially if the BSU do not lie exactly parallel to the alumina faces. As the objective aperture is displaced along the 002 ring in the SAD pattern, bright domains become dark whereas

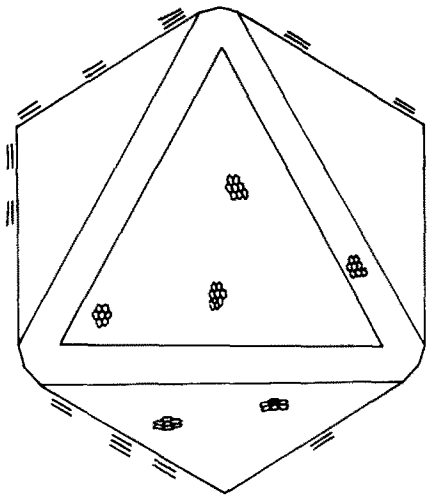

FIG. 7. Schematic representation of an incomplete shell of carbonaceous matter around alumina single crystals.

others light up around the alumina contours.

The assumption of a shell of carbonaceous BSU lying more or less flat on the alumina single crystal faces (Fig. 7) has to be discussed and confirmed by other experiments since the occurrence of bright domains decorating the outlines of the alumina crystal can be due to two kinds of spurious effect: first a contribution of the supporting film itself made of amorphous carbon; then a parasitic contribution of either $111_{Al_2O_3}$-scattered beams despite their very low intensity.

(1) The observations were repeated by using self-supported samples: poisoned catalyst deposited on perforated carbon films (microgrids). The withdrawal of all the supporting carbon does not change the images.

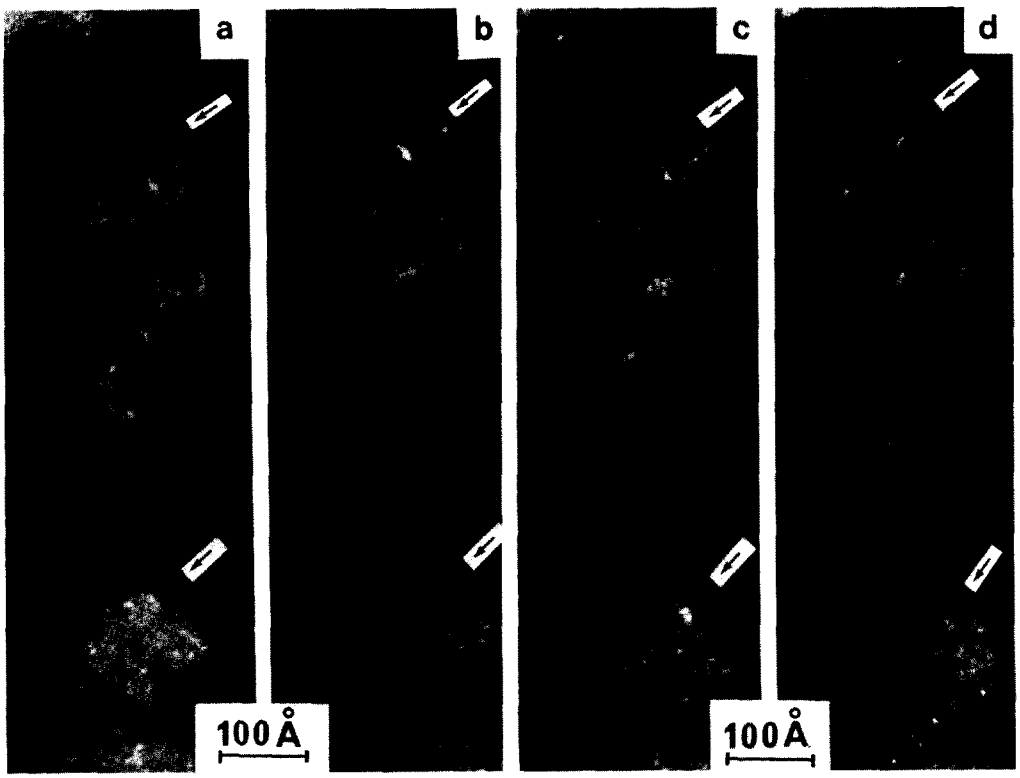

FIG. 8. Dark-field images of a catalyst containing 6.8% of carbon self-supported (deposited on a microgrid). (a) 0.20-$Å^{-1}$ aperture centered on 0.26 $Å^{-1}$ (corresponding to 3.85 Å). (b) Aperture centered on 0.30 $Å^{-1}$ (corresponding to 3.35 Å). (c) The aperture centered on 0.34 $Å^{-1}$ (corresponding to 2.94 Å). (d) Aperture centered on 0.40 $Å^{-1}$ (corresponding to 2.25 Å).

Thus there is no artefact due to the carbon supporting film.

(2) Two kinds of experiments were carried out for either minimizing or withdrawing the contribution of $111_{Al_2O_3}$ to DF images.

A first series of micrographs was taken by displacing radially the 0.20-$Å^{-1}$ aperture from the vicinity of the incident beam to $220_{Al_2O_3}$ (see Fig. 1). By doing so, the aperture lets through first $111_{Al_2O_3}$ and 002_{carbon}, then $111_{Al_2O_3}$, $220_{Al_2O_3}$, and mainly 002_{carbon}, and finally 002_{carbon} and $220_{Al_2O_3}$. Figure 8 illustrates the images corresponding to four positions of the aperture. Though the bright-domain patterns are the same in all the micrographs, the number of bright domains changes from one to the other. This is because first the piled-up aromatic structures are known to have usually widely spread interlayer spacing values (*7*), and then because the particle is self-supported, its orientation changes slightly relative to the incident beam during the series of exposures. This explains why the bright domains indicated by an arrow tend to vanish from a to b, then to light up again in c more than in d. Despite this, it is clear that the same bright domains can be seen in all the four micrographs. Since the 002-scattered beam of carbon represents the only common feature to the four micrographs, the bright dots common to all of them are necessarily carbon BSU. It has to be considered also that usually in alumina dark-field images, the entire single crystal is lit up (see Fig. 2). This gives entirely different images containing bright domains about 30–80 Å in size instead of 10 Å.

In the second series of experiments, a 0.1-$Å^{-1}$-size aperture was used for DF imaging (small black circle in Fig. 1). This aperture lets through only the 002-scattered beam of carbon. The resolution of the 0.20-$Å^{-1}$ aperture is about 7–8 Å while the resolution of the 0.1-$Å^{-1}$ aperture is only about 20 Å. The evaluation of the size of the bright domains (BSU) is thus no longer valid since they are smaller than the optimum possible resolution. Nevertheless, carbon BSU are still revealed with certainty (Figs. 9a, b). They appear as diffuse bright domains about 20 Å in size. Since the aperture intersects then the scattered beams of BSU misoriented only by a ±11° twisting instead of a ±22° one, a smaller number of domains appear bright. However, they always decorate preferably the

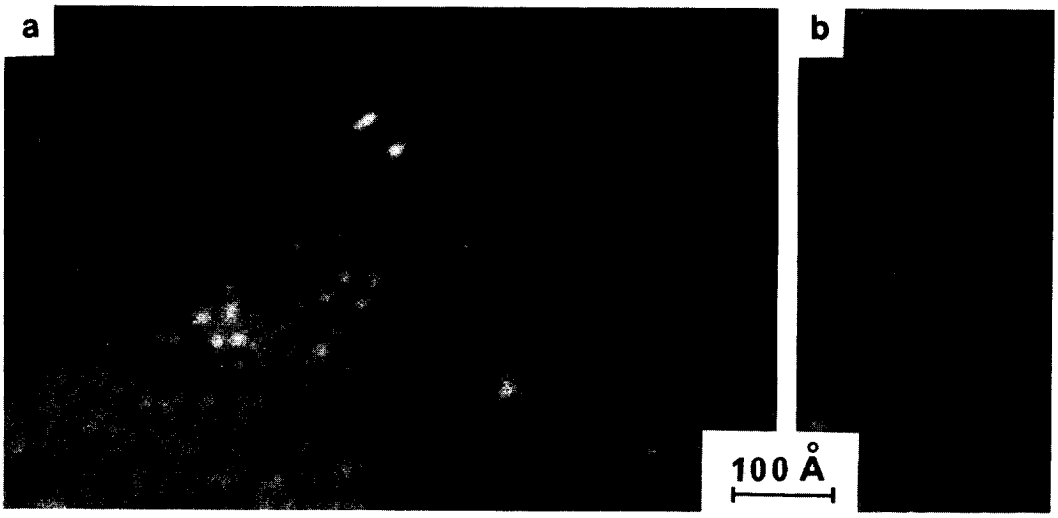

FIG. 9. The 002 carbon dark field of a self-supported catalyst containing 6.8% of carbon. Objective aperture 0.1-$Å^{-1}$. (a, b) Details from different micrographs.

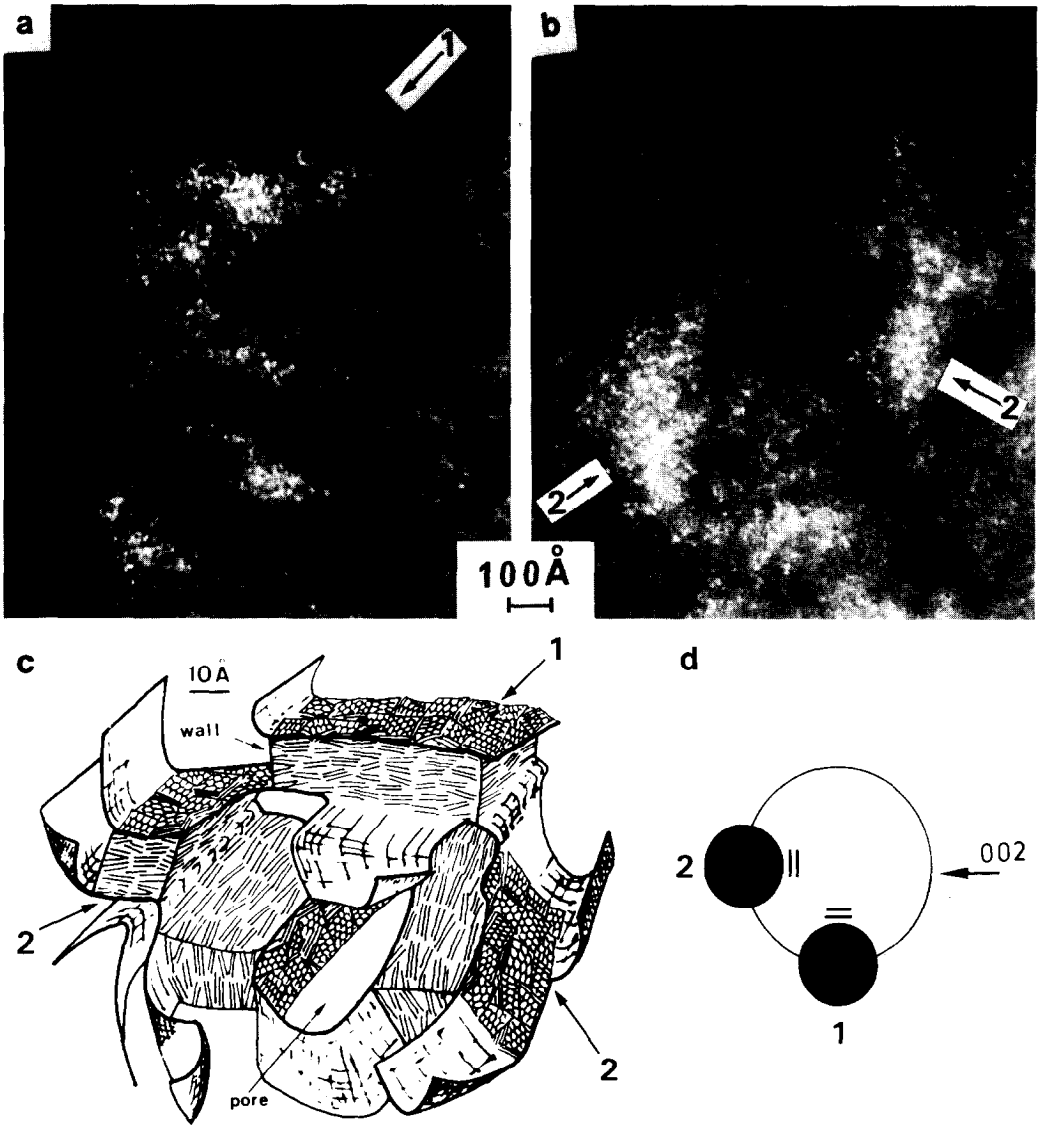

FIG. 10. Porous carbon particle observed in a catalyst containing 6.8% of carbon. (a, b) The 002 carbon dark field. (a) Corresponds to the aperture in the position numbered 1 in (d). (b) Corresponds to the position numbered 2. (c) Model of porous carbon. (d) Positioning of the aperture in the SAD pattern.

outlines of alumina crystals. These data demonstrate well the occurrence of carbonaceous matter.

Carbonaceous Particles

The BSU units can be fixed not only on alumina crystals but can also gather into aggregates forming carbon particles such as that indicated by an arrow in Fig. 6a. In 002 carbon DF, the bright domains are gathered into clusters (Figs. 10a and b) separated by dark areas. Such images are similar to those found in carbonaceous matter prepared by softening or from solid organic precursors (*6*, *7*). A complete exploration of the carbon reciprocal space including 002 DF micrographs leads us to imagine the porous model sketched in Fig. 10c and detailed in

other publications (*6, 7*). It is based mainly on the fact that for the position of the aperture numbered 1 in the SAD pattern of Fig. 10d, the clusters of bright dots of Fig. 10a correspond to the part of the pore wall numbered 1 (Fig. 10c), whereas the position numbered 2 corresponds to the pore wall numbered 2 (Fig. 10b). The molecular orientation extent, i.e., the size of the pore wall, is the size of the clusters of bright domains numbered 1 and 2 in Figs. 10a and b. It is about 500 Å in this case. It is not very different from that of the hydrogen-rich precursors studied in the laboratory (*6, 7*).

CONCLUSION

The model roughly sketched in Fig. 7, showing the formation of more or less incomplete shells of carbonaceous BSU on the alumina crystals, can be considered as valid and fits well with the data of the present paper. Each BSU is a stack of 2 or 3 aromatic planar ring structures less than 12 rings (less than 10 Å in size) lying approximately flat on the alumina crystal face. The exact diameter of the aromatic structures cannot be defined more precisely first because of the limiting value of the resolution. The size of each aromatic layer stack can be smaller or equal to the resolution value. Then each stack can be surrounded by an unknown amount of nonaromatic functional groups that the TEM cannot see and which may enlarge considerably the size of the real carbonaceous individual units. This may also increase the misorientation of the aromatic layer planes relative to the alumina crystal, acting as a support. As an increasing quantity of such carbon units is deposited on alumina faces, the poisoning effect can be expected to increase. Pt is supposed to play an important part in the creation of intermediates for coke formation so that the small BSU units of coke are formed in the interface. Then they are deposited indifferently on any available faces of the alumina crystals similarly to pyrocarbon deposits (*11*). Hence no special relationship is to be expected between Pt and the carbon deposit and carbon is deposited everywhere on alumina.

The porous carbon particles individualized in the catalyst probably play an insignificant role in poisoning since they are able to cover only a negligible amount of the total catalyst surface.

ACKNOWLEDGMENTS

We wish to thank Jeanne Ayache and Fouad Bensaïd of the Marcel Mathieu Laboratory who did part of the experimental work. One of us (R. C.) wishes to acknowledge a Fellowship awarded under the Argentina–France cultural agreement which made possible his stay in Orléans.

REFERENCES

1. Davis, S. M., and Somorjai, G. A., *J. Catal.* **65,** 78 (1980).
2. Gates, B. C., Katzer, J. R., and Schuit, G. C. A., "Chemistry of Catalytic Processes," p. 287. McGraw–Hill, New York, 1979.
3. Castro, A. A., Scelza, O. A., Benvenuto, E. R., Baronetti, G. T., and Parera, J. M., "Proceedings, 6th Ibero-American Symposium on Catalysis (Rio de Janeiro, 1978)," Paper 55.
4. Benson, J. E., and Boudart, M., *J. Catal.* **4,** 704 (1965).
5. Sad, M. R., Figoli, N. S., Bettramini, J. N., Jablonski, E. L., Lazzaroni, R. A., and Parera, J. M., *J. Chem. Technol. Biotechnol.* **30,** 374 (1980).
6. Oberlin, A., Terrière, G., and Boulmier, J. L., *Tanso* part I **80,** 29; part II **83,** 153 (1975).
7. Oberlin, A., Boulmier, J. L., and Villey, M., "Kerogen" (B. Durand, Ed.), Chap. 7, p. 191. Technip, Paris, 1980.
8. Hirsch, P. B., Howie, A., Nicholson, R. B., Pashley, D. N., and Whelan, M. J., "Electron Microscopy of Thin Crystals," p. 353. Butterworths, London, 1971.
9. Donnay, S. D. H., and Harker, D., *Amer. Mineral.* **22,** 446 (1937).
10. Rooksby, H. P., *Trans. Brit. Ceram. Soc.* **28,** 399 (1927).
11. Bokros, J. C., *in* "Chemistry and Physics of Carbon" (P. Walker, Jr., Ed.), Vol. 5, p. 1. Dekker, New York, 1969.